The Astrophysical Journal, 591:526–539, 2003 July 10
© 2003. The American Astronomical Society. All rights reserved. Printed in U.S.A.

THE SUNYAEV-ZELDOVICH EFFECT SIGNATURE OF EXCESS ENTROPY IN DISTANT, MASSIVE CLUSTERS

Ian G. McCarthy,[1] Gilbert P. Holder,[2] Arif Babul,[1,3] and Michael L. Balogh[4]

Received 2002 October 2; accepted 2003 March 21

ABSTRACT

Studies of cluster X-ray scaling relations have led to suggestions that nongravitational processes, e.g., radiative cooling and/or "preheating," have significantly modified the entropy of the intracluster medium (ICM). For the first time, we test this hypothesis through a comparison of predicted thermal Sunyaev-Zeldovich (SZ) effect scaling relations with available data from the literature. One of the relations that we explore, in principle, depends solely on SZ effect observations, thus offering an X-ray–independent probe of the ICM. A detailed comparison of the theoretical relations with the largest compilation of high-z SZ effect data to date indicates that the presence of an entropy floor is favored by the data. Furthermore, the inferred level of that floor, $K_0 \gtrsim 300$ keV cm^2, is comparable to that found in studies of X-ray scaling relations of nearby massive clusters. Thus, we find no evidence for significant evolution of the entropy floor out to $z \sim 0.7$. We further demonstrate that the high-quality data to be obtained from the upcoming Sunyaev-Zeldovich Array (SZA) and the (soon to be) upgraded Owens Valley Radio Observatory (OVRO) array will open powerful new windows into the properties of the ICM. Specifically, the new measurements will allow for accurate measurements of the ICM entropy for even the most distant galaxy clusters.

Subject headings: cosmic microwave background — cosmology: theory — galaxies: clusters: general — X-rays: galaxies: clusters

1. INTRODUCTION

The failure of theoretical self-similar X-ray scaling relations to match observed trends has led to suggestions that important nongravitational processes, such as radiative cooling and/or "preheating," are significantly affecting the structure and appearance of the intracluster medium (ICM). Models and simulations of clusters that attempt to explicitly take into account the effects of cooling and/or heating produce clusters that have higher mean entropies ("excess" entropy) than those produced by models that neglect these processes. In some cases, the model clusters possess cores in their entropy profiles commonly referred to as the "entropy floor." The presence of this entropy floor, in turn, modifies the predicted X-ray scaling relations, bringing them into much closer agreement with the observed correlations (e.g., Kaiser 1991; Evrard & Henry 1991; Bower 1997; Balogh, Babul, & Patton 1999; Wu, Fabian, & Nulsen 2000; Bryan 2000; Tozzi & Norman 2001; Borgani et al. 2001; Voit & Bryan 2001; Babul et al. 2002; McCarthy, Babul, & Balogh 2002; Thomas et al. 2002; Voit et al. 2002; Davé, Katz, & Weinberg 2002; Lloyd-Davies, Bower, & Ponman 2002). Direct observational evidence for an "entropy floor" in nearby groups and low-mass clusters has been presented by Ponman, Cannon, & Navarro (1999) and Lloyd-Davies, Ponman, & Cannon (2000).

To date, only X-ray observations have yielded information about the entropy floor, but because the X-ray surface brightnesses of groups/clusters suffer the effects of cosmological dimming [the bolometric surface brightness scales as $(1+z)^{-4}$], both direct and indirect studies of the entropy floor via X-ray observations have generally been limited to low-redshift ($z \lesssim 0.2$) systems. An *independent* test of the entropy floor hypothesis, which could also provide information on *high-redshift* clusters and, therefore, the evolution of the nongravitational processes that give rise to the entropy floor, would be extremely useful. In a companion paper (McCarthy et al. 2003, hereafter MBHB03), we argued that a number of scaling relations based entirely or in part on the thermal Sunyaev-Zeldovich (SZ) effect (Sunyaev & Zeldovich 1970, 1980) observables can, potentially, be used for both of these purposes. Our analysis indicated that even current SZ effect observational data from, for example, the Berkeley-Maryland-Illinois Association (BIMA) and Owens Valley Radio Observatory (OVRO) arrays and the Ryle Telescope, when compared to the predicted correlations, can be used to tell us something about the entropy floors of distant, massive clusters.

The primary focus of the present paper is a comparison of these predicted scaling relations with available data from the literature to determine if the SZ effect data favor the existence of an entropy floor and how the inferred level of the entropy floor compares with that required to explain local X-ray trends (which require $K_0 \gtrsim 300$ keV cm^2 for massive clusters; Tozzi & Norman 2001; Babul et al. 2002; McCarthy et al. 2002). *This is the first time that the SZ effect has been used as a probe of nongravitational entropy in galaxy clusters.*

A number of new SZ experiments, which will greatly improve the quality of the observations, are being planned or are already under construction. An additional goal of the present study, therefore, is to examine the efficacy of two of these experiments, the Sunyaev-Zeldovich Array (SZA) and the (soon to be) upgraded OVRO array, to constrain the properties of the excess entropy in distant clusters. By constructing and analyzing "mock" observations that take

[1] Department of Physics and Astronomy, University of Victoria, P.O. Box 3055, Victoria, BC V8P 1A1, Canada; mccarthy@beluga.phys.uvic.ca.
[2] School of Natural Sciences, Institute for Advanced Study, Princeton, NJ 08540.
[3] CITA Senior Fellow.
[4] Department of Physics, University of Durham, Science Laboratories, South Road, Durham DH1 3LE, UK.

explicit account of the expected instrumental responses of these arrays, we quantify the accuracy with which the level of the entropy floors of distant clusters can be inferred by future data as a function of redshift.

The present paper is outlined as follows. In § 2 we discuss and select available data from the literature. In § 3 we compare these data to our theoretical scaling relations. In § 4 we assess the ability of the upcoming SZA and upgraded OVRO array to probe the entropy floors of distant clusters. Finally, in § 5 we discuss and summarize our results. We assume $\Omega_m = 0.3$, $\Omega_\Lambda = 0.7$, and $H_0 = 75$ km s^{-1} Mpc^{-1} and work in physical units (e.g., $M_\odot$ rather than $h^{-1}\ M_\odot$) throughout the paper.

2. OBSERVATIONAL DATA

Observations of the SZ effect have advanced tremendously over the last decade or so, and routine high signal-to-noise ratio measurements of the effect are now being made with a variety of instruments (including both single-dish and interferometric experiments) at a variety of wavelengths (spanning radio down to the submillimeter). There now exist published data for some 30–40 clusters (e.g., Jones et al. 1993, 2003; Herbig et al. 1995; Carlstrom, Joy, & Grego 1996; Myers et al. 1997; Holzapfel et al. 1997, 2000; Hughes & Birkinshaw 1998; Pointecouteau et al. 1999, 2001, 2002; Patel et al. 2000; Joy et al. 2001; Mason, Myers, & Readhead 2001; Grego et al. 2001; Grainge et al. 2002a, 2002b; Reese et al. 2002; Cotter et al. 2002; LaRoque et al. 2003; Cantalupo et al. 2003). With this influx of new data, the sample is large enough to make statistically significant comparisons between observed and theoretically predicted SZ effect scaling relations. Such comparisons test our understanding of the ICM and clusters in general. In this section we compile and discuss cluster SZ effect data from the literature with the intention of comparing it to theoretically predicted scaling relations in § 3.

Of the 30–40 clusters that have published SZ effect data, we are particularly interested in those clusters that lie at high redshift. As already mentioned, the vast majority of studies on the *X-ray* scaling relations of clusters have been for low-redshift ($z \lesssim 0.2$) systems, but information on the entropy floors of more distant clusters is scant. Because the SZ effect is not subject to cosmological dimming, SZ effect scaling relations potentially offer a way of probing the nongravitational entropy of even the most distant galaxy clusters.

A search of the literature for high-redshift clusters with SZ effect data yields 22 different clusters in the range $0.14 \lesssim z \lesssim 0.78$, many of which were observed multiple times. The clusters are listed in Table 1 along with their redshifts, central Compton parameters (y_0), frequency-independent integrated SZ effect flux densities within the central $1'$ ($S_{\nu,\mathrm{arc}}/f_\nu$), and the bibliographic references (references in parentheses indicate that the cluster was observed multiple times). We are particularly interested in y_0 and $S_{\nu,\mathrm{arc}}/f_\nu$ because a number of scaling relations based on these two quantities are expected to be quite sensitive to the entropy floor level of galaxy clusters (see MBHB03).

Below we discuss how we extract y_0 and $S_{\nu,\mathrm{arc}}/f_\nu$ from the observational data. At present, it is not possible to directly measure either of these quantities. Observations of the SZ effect filter large-scale emission, while finite resolution smears out small-scale structures. As discussed in MBHB03, fitting a model (such as the isothermal β model; Cavaliere &

TABLE 1
SZ Effect Observational Data

Cluster (1)	z (2)	$\log y_0$ (3)	$\log(S_{\nu,\mathrm{arc}}/f_\nu)$ (4)	References (5)
A1413	0.143	$-3.794^{+0.053}_{-0.060}$	$0.954^{+0.062}_{-0.070}$	1, (2)
A2204	0.152	$-3.744^{+0.111}_{-0.150}$	...	3
A1914	0.171	-3.798	0.934	2
A2218	0.176	$-3.862^{+0.056}_{-0.081}$	$0.922^{+0.060}_{-0.086}$	1, (2)
A665	0.182	$-3.864^{+0.081}_{-0.100}$	$0.939^{+0.084}_{-0.104}$	1
A1689	0.183	$-3.489^{+0.029}_{-0.027}$	$1.169^{+0.038}_{-0.036}$	1
A520	0.199	$-3.906^{+0.058}_{-0.067}$	$0.914^{+0.065}_{-0.075}$	1
A2163	0.203	$-3.448^{+0.031}_{-0.033}$	$1.363^{+0.034}_{-0.036}$	1, (4), (5)
A773	0.217	$-3.626^{+0.052}_{-0.059}$	$1.132^{+0.080}_{-0.103}$	1, (2), (6)
A2261	0.224	$-3.497^{+0.048}_{-0.054}$	$1.137^{+0.085}_{-0.087}$	1
A1835	0.253	$-3.328^{+0.029}_{-0.027}$	$1.146^{+0.048}_{-0.050}$	1, (7)
A697	0.282	$-3.577^{+0.052}_{-0.052}$	$1.179^{+0.082}_{-0.091}$	1, (2)
A611	0.288	$-3.795^{+0.066}_{-0.066}$	$0.807^{+0.141}_{-0.179}$	1
Zw 3146	0.291	$-3.792^{+0.066}_{-0.077}$	...	3
A1995	0.319	$-3.717^{+0.032}_{-0.037}$	$0.943^{+0.092}_{-0.125}$	1
MS 1358.4+6245	0.327	$-3.832^{+0.047}_{-0.053}$	$0.720^{+0.083}_{-0.090}$	1
A370	0.375	$-3.628^{+0.154}_{-0.083}$	$1.145^{+0.204}_{-0.180}$	1
RX J2228+2037	0.421	-3.620	1.024	8
RX J1347.5−1145	0.451	$-3.130^{+0.037}_{-0.040}$	$1.245^{+0.069}_{-0.072}$	1, (9), (10)
Cl 0016+16	0.546	$-3.632^{+0.035}_{-0.038}$	$1.056^{+0.054}_{-0.059}$	1, (11), (12)
MS 0451.6−0305	0.550	$-3.571^{+0.027}_{-0.031}$	$1.041^{+0.076}_{-0.091}$	1
MS 1137.5+6625	0.784	$-3.814^{+0.048}_{-0.055}$	$0.608^{+0.243}_{-0.365}$	1, (13)

Note.—$S_{\nu,\mathrm{arc}}/f_\nu$ expressed in mJy.

References.—(1) Reese et al. 2002. (2) Jones et al. 2003. (3) Holzapfel 1996. (4) Holzapfel et al. 1997. (5) Lamarre et al. 1998. (6) Saunders et al. 2003. (7) Mauskopf et al. 2000. (8) Pointecouteau et al. 2002. (9) Pointecouteau et al. 2001. (10) Komatsu et al. 1999. (11) Grainge et al. 2002a. (12) Hughes & Birkinshaw 1998. (13) Cotter et al. 2002.

Fusco-Femiano 1976, 1978) to the SZ effect data provides a method for effectively removing these effects and estimating y_0 and $S_{\nu,\mathrm{arc}}/f_\nu$, but it should be kept in mind that such quantities are inferred and model dependent. Provided that the smallest angular scale resolved is comparable to the typical scale over which the cluster varies, the estimated central Compton parameter will be reliable, while inferred flux densities will be suspect when extrapolated beyond the filtering scale of the observations. For current interferometric observations (such as those obtained with the BIMA and OVRO arrays and the Ryle telescope), the highest angular resolution for SZ measurements is typically smaller than the core radius of the cluster ($\sim 30''$), while the large-scale filtering normally becomes important on scales larger than about $2'$. Therefore, it can be expected that the inferred values of y_0 and $S_{\nu,\mathrm{arc}}/f_\nu$ (the flux density within the central $1'$) should be accurate.

To calculate the total frequency-independent SZ effect flux density within the central $1'$ for each of these clusters, we must reconstruct each of the SZ effect "surface brightness" profiles, $y(\theta)$. The majority of the clusters listed in Table 1 were modeled using the spherical isothermal β model. In this model, the ICM is assumed to be isothermal and has a density distribution described by

$$n_e(r) = n_{e0}\left(1 + \frac{r^2}{r_c^2}\right)^{-3\beta/2}, \tag{1}$$

where n_{e0} is the central electron density, r_c is the cluster core radius, and β is the power-law index. This leads to an SZ effect surface brightness profile

$$y(\theta) = y_0\left(1 + \frac{\theta^2}{\theta_c^2}\right)^{1/2-3\beta/2}, \tag{2}$$

where $y(\theta)$ is the Compton parameter evaluated at a projected position $\theta = r/D_a$ from the cluster center and is proportional to the integrated pressure along the line of sight through the cluster. In addition, $\theta_c = r_c/D_a$ (D_a is the angular diameter distance).

The central Compton parameters, y_0, are converted from the central SZ effect temperature decrements (references are given in col. [5]) using the relation

$$\frac{\Delta T_0}{T_{\mathrm{CMB}}} = y_0\left(\frac{x}{\tanh x/2} - 4\right), \tag{3}$$

where ΔT_0 is the central SZ effect temperature decrement and $x = h\nu/kT_{\mathrm{CMB}}$ is the dimensionless frequency (T_{CMB} is the temperature of the present-day cosmic microwave background, 2.728 K [Fixsen et al. 1996], and ν is the observing frequency). We ignore the complication of relativistic effects, which only modify the Compton parameter of the hottest clusters by a few percent (Itoh, Kohyama, & Nozawa 1998; Nozawa et al. 2000).

We use the best-fit β model parameters (y_0 [ΔT_0], β, and θ_c) from the literature (discussed below) to reconstruct $y(\theta)$. The surface brightnesses are then numerically integrated within the central $1'$ (the result is symbolized by y_{int}) via

$$y_{\mathrm{int}}(\leq \theta = 1') = 2\pi \int_0^{\theta=1'} y(\theta')\theta'\, d\theta' \tag{4}$$

and, finally, converted into a frequency-independent flux density through

$$\frac{S_{\nu,\mathrm{arc}}}{f_\nu} = y_{\mathrm{int}}\left[\frac{2(kT_{\mathrm{CMB}})^3}{(hc)^2}\right], \tag{5}$$

where f_ν is a function of the dimensionless frequency x and is defined in MBHB03.

Ideally, the three β model parameters would be determined by fitting the model to the SZ effect data. However, current SZ effect data cannot tightly constrain these parameters when all three are left to vary independently (e.g., Carlstrom et al. 1996; Grego et al. 2000, 2001; Pointecouteau et al. 2001, 2002). This problem is often circumvented by adopting the best-fit values of β and θ_c (the "shape" parameters) determined from fitting to the *X-ray* surface brightness profile of the cluster and leaving only the normalization, y_0, to be determined from fitting to the SZ effect data (e.g., Pointecouteau et al. 1999, 2001, 2002; Patel et al. 2000; Jones et al. 2003; LaRoque et al. 2003; Grainge et al. 2002b). In the case of clusters with moderate redshifts (which is a good description of most of the clusters in Table 1), X-ray data still provide better constraints on β and θ_c than do SZ effect data. Thus, in the cases of A1914 and RX J2228+2037, we use the X-ray–determined values of these parameters to calculate $S_{\nu,\mathrm{arc}}/f_\nu$. However, a better approach is to use all available data (both the SZ effect and X-ray data) to constrain these parameters. In estimating the Hubble constant from a sample of 18 distant clusters, Reese et al. (2002) did just this. The shape parameters, central X-ray surface brightness, and y_0 were all determined simultaneously by using a joint maximum likelihood analysis of both SZ effect and X-ray data. Because their sample is large (in fact, it is the largest sample of SZ effect clusters observed to date) and homogeneously analyzed and their method takes advantage of all ICM imaging data, we preferentially use the values of y_0, β, and θ_c measured by Reese et al. (2002) when multiple measurements for a particular cluster are available (which is the case for roughly half of the clusters listed in Table 1). We note that the agreement between different studies is reasonably good (estimates of y_0 differ by $\lesssim 20\%$ from study to study; e.g., Holzapfel et al. 1997; Jones et al. 2003). Using the best-fit parameters of Reese et al. (2002), we calculate $S_{\nu,\mathrm{arc}}/f_\nu$ for these 18 clusters. Published values for the shape parameters of the two remaining clusters in Table 1, A2204 and Zw 3146, are not available.

To calculate the uncertainty associated with the SZ effect flux density, we vary y_0, β, and θ_c within their allowable ranges (each of the three free parameters has an associated statistical uncertainty) to determine the maximum and minimum possible flux density of the cluster. This method actually *overestimates* the uncertainty associated with the flux density as there is a known correlation between the β and θ_c parameters for current SZ effect data (e.g., Grego et al. 2000, 2001).

We are also interested in mapping out correlations between SZ effect and X-ray observables. In Table 2 we list the total dark matter masses within r_{500} [$M(r_{500})$], the mean emission-weighted gas temperatures (T_{X}), and bolometric X-ray luminosities (L_{X}) of these clusters. We also list whether the cluster has a sharp centrally peaked X-ray surface brightness profile, which presumably indicates the presence of a cooling flow (CF indicates that the cluster is a "cooling flow cluster," while NCF indicates that it is not;

TABLE 2
X-Ray Observational Data

Cluster (1)	$\log M(r_{500})$ (2)	$\log T_X$ (3)	$\log L_X$ (4)	Type (5)	References (6)
A1413	14.86	$0.929^{+0.062}_{-0.043}$	$45.082^{+0.018}_{-0.018}$	CF	1, 2, 3
A2204	14.88	$0.964^{+0.104}_{-0.055}$	45.407	CF	1, 2, 3
A1914	...	$0.934^{+0.018}_{-0.020}$	...	NCF	4
A2218	14.73	$0.839^{+0.030}_{-0.033}$	$44.974^{+0.018}_{-0.018}$	NCF	1, 3, 5
A665	14.83	$0.944^{+0.042}_{-0.047}$	$45.124^{+0.013}_{-0.013}$	NCF	1, 3, 6
A1689	15.06	$1.000^{+0.049}_{-0.036}$	$45.423^{+0.010}_{-0.010}$	CF	1, 2, 3
A520	14.75	$0.921^{+0.038}_{-0.036}$	45.070	NCF	1, 2, 3
A2163	15.11	$1.090^{+0.044}_{-0.041}$	45.732	NCF	1, 3, 6
A773	...	$0.968^{+0.016}_{-0.016}$	45.278	NCF	2, 7
A2261	...	$1.037^{+0.188}_{-0.098}$	45.447	CF	2, 8
A1835	...	$0.991^{+0.092}_{-0.062}$	45.725	CF	2, 7
A697	...	$1.009^{+0.074}_{-0.090}$	...	NCF	9
A611	...	$0.836^{+0.029}_{-0.030}$	...	CF	9
Zw 3146	14.91	$1.053^{+0.180}_{-0.119}$	45.525	CF	1, 2, 7
A1995	...	$1.016^{+0.053}_{-0.053}$	$45.241^{+0.010}_{-0.010}$	CF	10, 10
MS 1358.4+6245	14.81	$0.875^{+0.289}_{-0.097}$	$45.093^{+0.014}_{-0.014}$	CF	1, 2, 10
A370	...	$0.848^{+0.031}_{-0.032}$	$45.236^{+0.010}_{-0.010}$	NCF	9, 10
RX J2228+2037	...	...	...	NCF	
RX J1347.5−1145	...	$1.422^{+0.112}_{-0.272}$	$46.093^{+0.003}_{-0.003}$	CF	2, 10
Cl 0016+16	...	$0.911^{+0.041}_{-0.045}$	...	NCF	9
MS 0451.6−0305	...	$0.908^{+0.041}_{-0.045}$	45.610	NCF	11, 11
MS 1137.5+6625	...	$0.799^{+0.027}_{-0.028}$	45.158	NCF	11, 11

Note.—Masses, temperatures, and bolometric luminosities are expressed in $M_\odot$, keV, and ergs s^{-1}, respectively.

References.—(1) Ettori & Fabian 1999. (2) Allen 2000. (3) White et al. 1997. (4) Jones et al. 2003. (5) Machacek et al. 2002. (6) Markevitch & Vikhlinin 2001. (7) Mushotzky & Scharf 1997. (8) Allen & Fabian 1998. (9) White 2000. (10) Novicki et al. 2002. (11) Vikhlinin et al. 2002.

Allen 2000; Reese et al. 2002), and the references for $M(r_{500})$, T_X, and L_X, respectively. Below we discuss the X-ray data in columns (2)–(4) of Table 2.

For the total dark matter masses within r_{500} (col. [2]), we turn to the study of Ettori & Fabian (1999). By constructing X-ray surface brightness profiles that are based on the "universal" dark matter density (NFW) profile (Navarro, Frenk, & White 1997) and comparing these to data from *ROSAT*, these authors were able to model the underlying dark matter density for nine of the clusters listed in our Table 1. We use their best-fit parameters (listed in their Tables 1 and 2) to recover the dark matter density profiles of these clusters. We take care to properly scale these parameters for our assumed cosmology. We then integrate the density profiles out to r_{500} to determine the total dark matter mass within that radius. We are unable to estimate the uncertainty on the masses, as there is no reported uncertainty for the best-fit NFW parameters of these clusters.

The most recently determined values for the ICM temperatures of these clusters are also listed in Table 2 (col. [3]). Of the 21 clusters with reported temperatures, 16 have temperatures determined via fitting to *ASCA* X-ray spectral data (Allen 2000; White 2000; Novicki, Sornig, & Henry 2002; Jones et al. 2003) and five have measurements based on fits to new *Chandra* X-ray spectral data (Markevitch & Vikhlinin 2001; Machacek et al. 2002; Vikhlinin et al. 2002). The cluster RX J2228+2037 does not have a temperature deduced from X-ray spectral analysis, although its central temperature was estimated by a combined analysis of X-ray and SZ effect *imaging* data (Pointecouteau et al. 2002). In the interest of homogeneity, however, we do not include this cluster in our analysis of scaling relations involving the emission-weighted gas temperatures because it is unclear how the reported temperature is related to the X-ray emission-weighted temperature. For the clusters that have sharp centrally peaked X-ray surface brightnesses and apparently harbor massive cooling flows (Allen 2000; Reese et al. 2002; see col. [5]), we use cooling flow–corrected temperatures. The temperatures were corrected by fitting the X-ray spectra with a multiphase plasma model that explicitly takes into account the cooler emission from the cluster core (Allen 2000). We note that for the clusters in this sample, cooling flow correction only slightly increases the temperature of a cluster (by about 10% or 1 keV) and does not significantly affect our results.

Finally, column (4) lists the bolometric X-ray luminosities of these clusters. We preferentially select data that have published uncertainties (e.g., White, Jones, & Forman 1997; Novicki et al. 2002). For data without published uncertainties, we select on the basis of X-ray satellite in the following order: *Chandra*/*XMM-Newton*, *ASCA*, and *ROSAT*/*Einstein*. Of the 17 clusters that have published bolometric luminosities, seven were determined using *Einstein* imaging data (White et al. 1997), one was determined using *ROSAT* imaging data (Allen & Fabian 1998), seven were determined using *ASCA* imaging data (Mushotzky & Scharf 1997; Novicki et al. 2002), and two were determined using new *Chandra* imaging data (Vikhlinin et al. 2002). Unfortunately, cooling flow–corrected luminosities (which normally entail excising the central 100–200 kpc of the CF cluster; e.g., Markevitch 1998; Vikhlinin et al. 2002) were not available for the CF clusters in Table 2.

Tables 1 and 2 comprise the largest compiled sample of high-redshift SZ effect clusters to date. We note that the

current compilation is not statistically complete or homogeneous, as discussed in Reese et al. (2002). Clusters with bright radio point sources were avoided, for the most part, and targets were selected primarily on the basis of X-ray luminosity. This compilation cannot be simply defined as being flux limited or luminosity limited, for example, and it is not complete over the range of redshifts studied. Without a simple selection function it is difficult to assess possible systematic effects that could be introduced by not having a sample that adequately reflects the demographics of the general population of galaxy clusters.

Below we compare the data in Tables 1 and 2 to our theoretically predicted scaling relations (see Table 1 of MBHB03) and attempt to determine if the data require an entropy floor (similar to that of X-ray data of nearby clusters) and, if so, what is the level of that entropy floor.

3. RESULTS

3.1. *Comparing Theory to Observations*

A detailed analysis of how the presence of excess entropy alters SZ effect scaling relations was presented in MBHB03. These relations were derived using the entropy injection (preheated) models developed by Babul et al. (2002). Following standard practice, we fitted simple power-law models to the theoretical scaling relations. Since a number of the relations were quite sensitive to redshift and existing SZ effect data span a wide range in z (see Table 1), we fitted power-law models that were an explicit function of both redshift and entropy floor level (K_0) to the theoretical relations; i.e., for arbitrary cluster parameters X and Y (e.g., y_0 and T_X)

$$\log_{10} Y = a(K_0, z) \log_{10} X + b(K_0, z) \ . \qquad (6)$$

With these relations, it is possible to quickly and accurately compute how various cluster properties scale with the SZ effect of the Babul et al. (2002) model clusters at any redshift between $0.1 \lesssim z \lesssim 1$ and with any entropy floor in the range 100 keV cm^2 $\lesssim K_0 \lesssim$ 700 keV cm^2 (see Table 1 of MBHB03). This is the only way a fair comparison can be made between the existing data and the theoretical models.

We compare the theoretical scaling relations to the observational data compiled in Tables 1 and 2 with a χ^2 statistic

$$\chi^2 = \sum_{i=1}^{N} \frac{[\log Y_i - a(K_0, z) \log X_i - b(K_0, z)]^2}{\sigma_{Y_i}^2 + a(K_0, z)^2 \sigma_{X_i}^2} \ , \qquad (7)$$

where $\sigma_{Y_i}^2$ and $\sigma_{X_i}^2$ are the measurement errors in log-space and are estimated by multiplying the measurement errors in linear-space by the weighting factors $(Y_i \log e)^{-1}$ and $(X_i \log e)^{-1}$, respectively (see, e.g., Press et al. 1992).

We specify the optically determined redshifts for each of the clusters and then determine the best-fit value of entropy floor level, K_0, by minimizing the χ^2 (assuming that the value of K_0 is the same for all clusters). Unless stated otherwise, quoted error bars are for the 95.4% (2 σ) confidence level (corresponding to $\Delta\chi^2 = 4$). We assess the quality of the fit by calculating the reduced χ^2 (χ_ν^2). For the self-similar model (whose scaling relations depend on z only; i.e., there are no free parameters), we calculate the χ^2 and χ_ν^2 and compare this with that of the best-fit entropy floor model.

Below we examine seven different scaling relations involving the two primary SZ effect observables (the central Compton parameter and the integrated flux density). First, we explore the trend that exists between the two SZ effect observables. This is an extremely interesting test since it can potentially be measured entirely independent of X-ray observations. In fact, in § 4 we show that future data from the SZA and the upgraded OVRO array will allow one to constrain the central entropy distribution of clusters all the way out to $z \sim 2$ using this relation. The next two trends that we study, between the two SZ effect observables and the mass of a cluster, are also interesting because they too can potentially be measured independent of X-ray observations. Aside from X-ray observations, one can estimate the mass of a cluster via gravitational lensing or through galaxy velocity dispersion measurements. We expect that the y_0-$M(r_{500})$ relation, in particular, will be very sensitive to the presence of excess entropy. Finally, the four remaining correlations that we look at are between the two SZ effect observables and the two primary X-ray observables, i.e., the mean emission-weighted temperature (T_X) and the bolometric luminosity (L_X). The correlations between the SZ effect observables and the cluster temperature are expected to be excellent probes of the central entropy of clusters, and, as such, we discuss these ahead of those involving L_X.

3.2. *An SZ Effect–only Relation*

We start by examining the correlation between the two SZ effect quantities, $S_{\nu,\mathrm{arc}}/f_\nu$ and y_0 (see Fig. 2 of MBHB03). Even though theoretical arguments suggest that this relation is not as sensitive to the presence of excess entropy as some of the other relations we will discuss later, it is by far the most interesting. As we already mentioned, this relation can potentially be measured entirely through SZ effect observations, offering a completely X-ray–independent probe of the intracluster gas. This is discussed in more detail below.

Fitting all 20 clusters in Table 1 for which we have estimates of both $S_{\nu,\mathrm{arc}}/f_\nu$ and y_0, we find a best-fit entropy floor level of $K_0 = 540^{+170}_{-165}$ keV cm^2 with $\chi_\nu^2 = 37.77/19 = 1.99$. A residual plot demonstrating the quality of our best-fit entropy floor model is presented in Figure 1 (*top panel*). The residuals from a comparison between the self-similar model and the data in Table 1 are presented in the bottom panel ($\chi_\nu^2 = 244.15/20 = 12.21$). Note that the residuals in the top panel are generally consistent with the zero line (indicating a relatively good fit), whereas the residuals in the bottom panel are systematically too high, indicating that the self-similar model predicts values of $S_{\nu,\mathrm{arc}}/f_\nu$ (for a fixed y_0) that are systematically lower than observed. This is equivalent to saying that the self-similar model predicts clusters that have SZ effect surface brightness profiles that are too centrally peaked. The entropy floor models are able to match the observations much better because the addition of an entropy floor flattens the pressure profiles of clusters (e.g., Fig. 1 of MBHB03), and since the SZ effect is proportional to the integrated line-of-sight pressure of the cluster, this leads to flatter surface brightness profiles.

There is little doubt that the best-fit entropy floor model provides a much better fit than the self-similar model to the observational data, but the best-fit entropy floor model itself does not provide a statistically acceptable fit to the data (note the high value of the χ_ν^2). However, the residuals in the top panel of Figure 1 clearly show two obvious

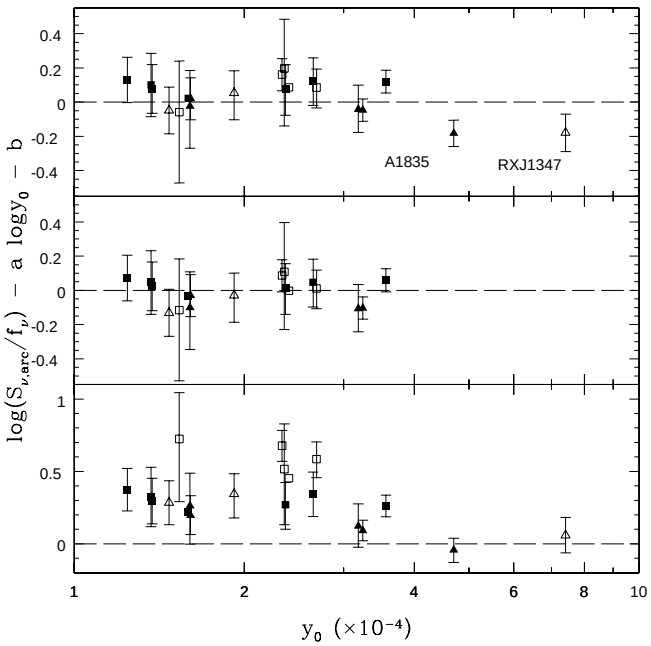


FIG. 1.—Residual plots for the $S_{\nu,\mathrm{arc}}/f_\nu$-$y_0$ relation. *Top:* Residuals from a comparison between the entropy floor model with $K_0 = 540$ keV cm^2 and the data in Table 1 ($\chi^2_\nu = 1.99$). *Middle:* Neglecting A1835 and RX J1347.5−1145 (for reasons discussed in the text) greatly improves the fit: $K_0 = 570$ keV cm^2 with $\chi^2_\nu = 0.99$. *Bottom:* Residuals from a comparison between the self-similar model and the data in Table 1 ($\chi^2_\nu = 12.21$). Filled symbols represent low-redshift ($z < 0.3$) clusters, open symbols represent high-redshift ($z > 0.3$) clusters, triangles represent cooling flow clusters, and squares represent non–cooling flow clusters. For clarity, error bars for the abscissa are not displayed.

outliers, A1835 and RX J1347.5−1145. Neglecting these two clusters, the quality of the fit to the whole sample is significantly improved: we find $K_0 = 575^{+150}_{-155}$ keV cm^2 with $\chi^2_\nu = 16.79/17 = 0.99$. The residuals for this fit are plotted in the middle panel of Figure 1. This result is consistent with that determined from studies of X-ray scaling relations of nearby massive clusters, which require $K_0 \gtrsim 300$ keV cm^2 (e.g., Tozzi & Norman 2001; Babul et al. 2002; McCarthy et al. 2002).

It is interesting that the two outliers, A1835 and RX J1347.5−1145, have extraordinarily large cooling flow mass deposition rates. Both apparently deposit several thousand solar masses of gas each year and are among the most massive cooling flow clusters known (Allen 2000). In fact, a closer inspection of the residuals reveals that there is a small systematic difference between cooling flow clusters (*triangles*) and non–cooling flow clusters (*squares*), even if one neglects these two outliers. While in principle the SZ effect should be less susceptible than the X-ray emission to the effects of cooling flows (because SZ effect is proportional to n_e, whereas the X-ray emission is proportional to n_e^2), recall that both of the SZ effect quantities used in Figure 1 were inferred through fitting to both X-ray and SZ effect data. Thus, the strong central surface brightness peaks present in the X-ray images of these cooling flow clusters will have an impact on the implied SZ effect observables. Excluding A1835 and RX J1347.5−1145, however, there is no statistical evidence for a difference in K_0 when fitting to the cooling flow and non–cooling flow clusters separately or to the whole sample. Therefore, it appears that only the most extreme cooling flow clusters could have significantly different entropy histories.

Because the sample in Table 1 is reasonably large and spans a wide range of redshifts, it is possible to use the catalog to get some idea of how the entropy floor level of clusters evolved with cosmic time. We split the sample up into two large redshift bins: (1) "low"-redshift clusters ($z < 0.3$) and (2) "high"-redshift clusters ($z > 0.3$). Fitting only the low-redshift clusters, we derive $K_0 = 505^{+220}_{-210}$ keV cm^2 ($\chi^2_\nu = 10.46/10 = 1.05$), which is consistent with the value derived from fitting to the entire sample. The high-redshift clusters, however, prefer a slightly elevated entropy floor with $K_0 = 640^{+205}_{-215}$ keV cm^2 ($\chi^2_\nu = 5.84/6 = 0.97$), although the difference between the low- and high-redshift clusters is not statistically significant. Thus, there is no good evidence that K_0 evolves significantly out to $z \sim 0.7$, at least on the basis of this test. A stronger test of this hypothesis will soon be possible, as the list of high-redshift clusters observed through the SZ effect is growing rapidly (Carlstrom and Joy and collaborators, for example, have now made detections in 21 clusters with $z > 0.45$; Reese et al. 2002).

Finally, to what extent the present $S_{\nu,\mathrm{arc}}/f_\nu$-$y_0$ relation studied here is independent of previous X-ray results is debatable. Both $S_{\nu,\mathrm{arc}}/f_\nu$ and y_0 were *inferred* by fitting a model to the SZ effect surface brightness profiles of clusters, and, furthermore, this surface brightness model (the isothermal β model) had two of its three free parameters constrained to be the same as that deduced from X-ray observations (Jones et al. 2003; Pointecouteau et al. 2002) or from X-ray and SZ effect observations (Reese et al. 2002). Yet, it is also clear that this test is different from any other scaling relation examined to date. Ideally, both $S_{\nu,\mathrm{arc}}/f_\nu$ and y_0 could be measured directly or, failing that, determined from fitting a model to only the SZ effect data. Current SZ effect data alone, however, cannot tightly constrain these quantities. In § 4 we show that the high-quality data to be produced by the upcoming SZA and the (soon to be) upgraded OVRO array will make it possible to accurately measure these quantities for massive clusters at virtually any redshift and without having to use any X-ray results.

3.3. *The SZ Effect–$M(r_{500})$ Relations*

The next set of scaling relations we examine are the SZ effect–cluster mass relations. Theoretical arguments suggest that these relations should be very sensitive to the presence of the entropy floor, at least when the SZ effect is measured near the cluster center (e.g., y_0). Interestingly, these trends can also potentially be measured independent of X-ray results. Future SZ effect observations will allow one to estimate y_0 and $S_{\nu,\mathrm{arc}}/f_\nu$ accurately purely through SZ effect surface brightness profiles (see § 4), while both strong lensing and weak lensing are increasingly being used to measure the mass profiles of clusters out to radii comparable in size to that of r_{500} (e.g., Clowe & Schneider 2001). At present, however, only a few of the clusters in our sample have been weighed using lensing.

In Figure 2 we plot the observed y_0-$M(r_{500})$ relation. This is superimposed on the predicted $z = 0.2$ y_0-$M(r_{500})$ relations for the self-similar model (*dotted line*) and the $K_0 = 100$ (*short-dashed line*), 300 (*long-dashed line*), 500 (*dot-dashed line*), and 700 keV cm^2 (*solid line*) entropy floor

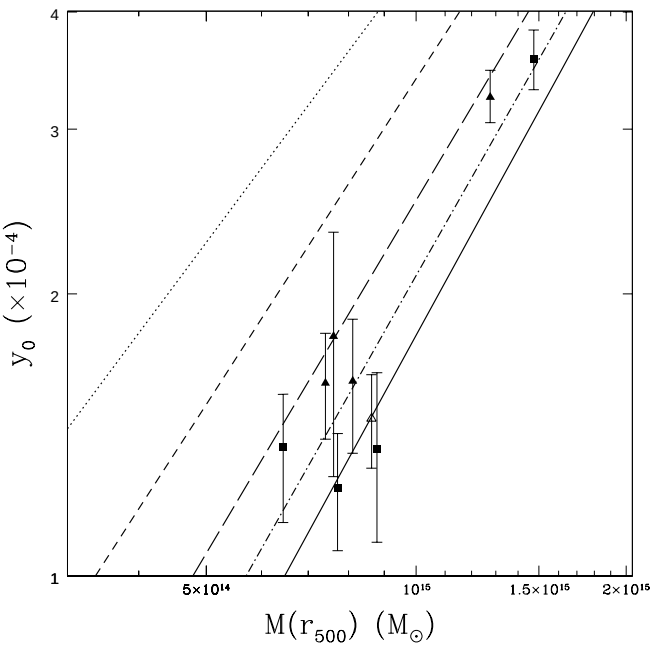


FIG. 2.—Observed and predicted y_0-$M(r_{500})$ relations. The symbols have the same meaning as in Fig. 1. The dotted, short-dashed, long-dashed, dot-dashed, and solid lines represent the self-similar and $K_0 = 100$, 300, 500, and 700 keV cm^2 entropy floor models, respectively.

models. Because the majority of the clusters with published masses in Tables 1 and 2 lie in a narrow redshift range around $z \sim 0.2$, it is possible to *qualitatively* compare the theoretical models to the data "by eye" before using the quantitative method outlined in § 3.1. A simple, neat, and fair qualitative comparison was not possible for the previous relation ($S_{\nu,\mathrm{arc}}/f_\nu$-$y_0$), as the data spanned a wide range of redshifts and because that relation is especially sensitive to z (S_ν scales as $1/D_a^2$).

By visual inspection of Figure 2, it is obvious that only the high entropy floor models ($K_0 \gtrsim 300$ keV cm^2) provide a reasonable fit to the observational data. In addition, the observed correlation does not seem to depend on the cooling flow status or redshift of the clusters, although the sample is far too small to make any robust conclusions to this effect. Fitting all nine clusters with the method outlined in § 3.1, our best-fit entropy floor level is $K_0 = 500^{+65}_{-65}$ keV cm^2 with $\chi^2_\nu = 8.02/8 = 1.00$. This is consistent with the results derived in § 3.2 and with X-ray observations of nearby massive clusters. A plot of the residuals between the data and the $K_0 = 500$ keV cm^2 model is shown in the left-hand panel of Figure 3. Also shown (*right-hand panel*) are the residuals of a comparison between the data and the self-similar model ($\chi^2_\nu = 376.05/9 = 41.80$). The residuals for the $K_0 = 500$ keV cm^2 model display a tight scatter about the zero line, while the residuals for the self-similar model indicate that y_0 is observed to be much lower [for a fixed value of $M(r_{500})$] than predicted by this model. The entropy floor models with $K_0 \sim 500$ keV cm^2 are able to provide a good match to the data because the addition of an entropy floor reduces the gas pressure near the centers of clusters (see MBHB03 for a detailed discussion). This, in turn, reduces the magnitude of y_0. The mass within r_{500}, however, is unaffected by the modification of the gas entropy.

Although the available y_0-$M(r_{500})$ data exhibit only a very small amount of scatter about the $K_0 \sim 500$ keV cm^2 relation (and the χ^2_ν indicates a very good fit), the estimated error bars on our best-fit value of K_0 from this relation are almost certainly too small. We say this because (1) we were unable to calculate any uncertainty for $M(r_{500})$ as there were no published error bars for the best-fit NFW parameters for the clusters in Figures 2 and 3, and (2) the sample is too small to get any kind of a handle on the systematic errors associated with the cluster masses. For example, estimates of cluster masses from gravitational lensing very often differ from those determined from X-ray data (sometimes by up to a factor of 2; e.g., Miralda-Escudé & Babul 1995; Wu &

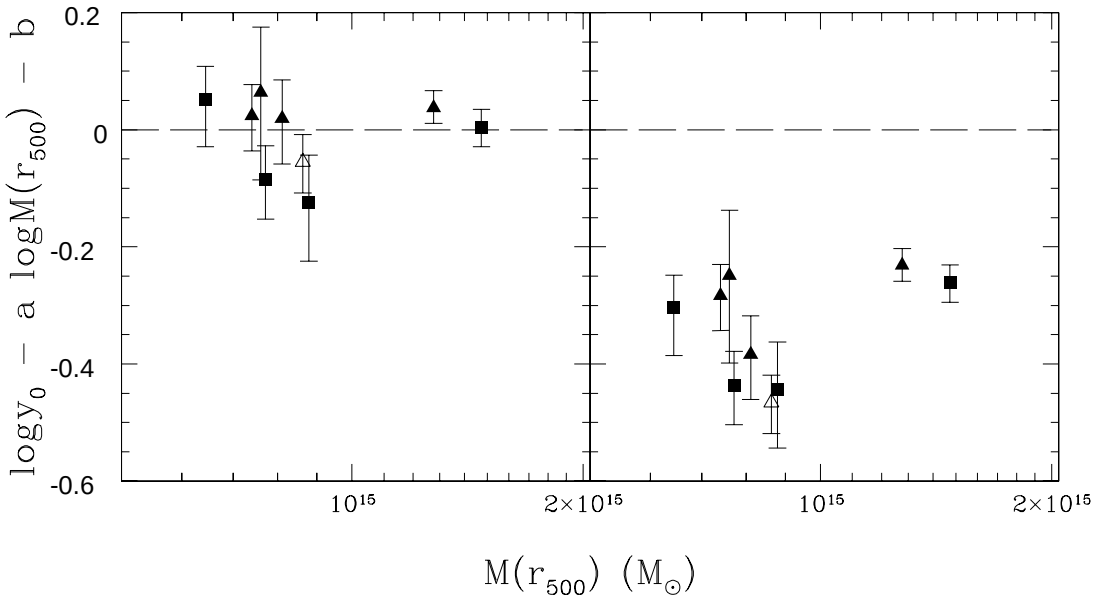


FIG. 3.—Residual plots for the y_0-$M(r_{500})$ relation. *Left:* Residuals from a comparison between the entropy floor model with $K_0 = 500$ keV cm^2 and the observational data ($\chi^2_\nu = 1.00$). *Right:* Residuals from a comparison between the self-similar model and the observational data ($\chi^2_\nu = 41.80$). The symbols have the same meaning as in Fig. 1. For clarity, error bars for the abscissa are not displayed.

Fang 1997; Ota et al. 2002), and it is not yet clear why this happens to be the case. There could be a systematic problem with the X-ray–determined masses (e.g., Allen 1998).

Aside from the y_0-$M(r_{500})$ relation, we also explore the $S_{\nu,\mathrm{arc}}/f_\nu$-$M(r_{500})$ trend. This trend could provide a consistency check of the results discussed immediately above. Unfortunately, the available SZ effect flux density–mass data do not constrain K_0. This is not completely unexpected since the $S_{\nu,\mathrm{arc}}/f_\nu$-$M(r_{500})$ relation is much less sensitive than the y_0-$M(r_{500})$ relation to the entropy floor level of clusters (MBHB03). Future data from, for example, the SZA will allow for much more precise determinations of the SZ effect flux densities of clusters, and we expect that the future $S_{\nu,\mathrm{arc}}/f_\nu$-$M(r_{500})$ relation will place much tighter constraints on K_0.

3.4. *The SZ Effect–T_X Relations*

Plotted in Figure 4 is the observed y_0-T_X relation. In addition to the observational data, we have also plotted the $z = 0.2$ (*thick lines*) and 0.5 (*thin lines*) theoretical relations. The various line types (e.g., solid, dotted) have the same meanings as in Figure 2. Again, because the theoretical relations are not a strong function of redshift, a preliminary visual comparison of the data and models is feasible.

First, it is clear that the data indicate that there is a fairly tight correlation between a cluster's central Compton parameter and its emission-weighted gas temperature. This correlation seems to hold true irrespective of whether the clusters have cooling flows or not. This may be expected since we have used cooling flow–corrected temperatures. However, even without this correction the data still exhibit a tight trend. For the clusters in this sample, cooling flow correction only slightly increases the temperature of a cluster (by about 10% or 1 keV) and, therefore, does not significantly affect the results. There is also a hint of a slight systematic difference in the y_0-T_X relations for low- and high-redshift clusters (*filled and open symbols, respectively*). In particular, the relation for the high-redshift clusters has a normalization that is slightly higher than that of the relation for low-redshift clusters (ignoring RX J1347, whose temperature is quite uncertain). This is discussed in more detail below.

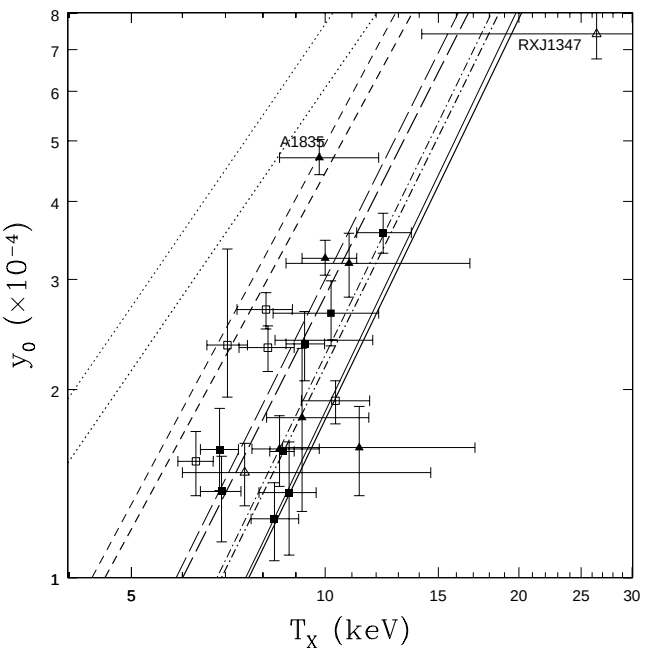


FIG. 4.—Observed and predicted y_0-T_X relations. The symbols have the same meaning as in Fig. 1. The dotted, short-dashed, long-dashed, dot-dashed, and solid lines represent the self-similar and $K_0 = 100$, 300, 500, and 700 keV cm^2 entropy floor models, respectively. Thin lines are for $z = 0.2$, and thick lines are for $z = 0.5$. As discussed in the text, the models with $K_0 \sim 300$ keV cm^2 provide the best description of the observations.

Comparing the various theoretical relations to the observational data, it is apparent that the standard self-similar model predicts a y_0-T_X relation that is a poor match to the data. In particular, the normalizations of the self-similar relations are roughly 2.5 times larger than observed (over the range 6 keV $\lesssim T_X \lesssim$ 12 keV). The entropy floor models with $K_0 \sim 300$ keV cm^2, on the other hand, provide a very good qualitative fit to the data. In MBHB03, we found that injecting the ICM with nongravitational entropy tends to decrease y_0 and, at the same time, increase T_X. This reduces the normalization of the predicted trend between these two quantities and, as is apparent from Figure 4, brings close agreement between theory and observations.

Fitting all 21 clusters in Tables 1 and 2 via the method outlined in § 3.1, we obtain a best-fit entropy floor of $K_0 = 300^{+80}_{-60}$ keV cm^2 with $\chi^2_\nu = 26.36/20 = 1.32$. The residuals of a comparison between the $K_0 = 300$ keV cm^2 entropy floor model and the self-similar model with the observation data are plotted in Figure 5. Note the striking separation between the residuals of the two models. Theoretically, the y_0-T_X relation is the most sensitive to the entropy floor level of any and all scaling relations that we have explored.

If we exclude A1835 and RX J1347.5−1145 from the fit, the entropy floor is essentially unchanged ($K_0 = 305^{+80}_{-65}$ keV cm^2), but the fit is improved ($\chi^2_\nu = 22.37/18 = 1.24$). In addition, we verify that splitting the sample by cooling flow status does not significantly modify the best-fit value of K_0. As mentioned above, there appears to be a slight difference in the normalizations of the y_0-T_X relations for low- and high-redshift clusters. Is this difference significant? If we restrict the fit to low-redshift ($z < 0.3$) clusters only, we find a best-fit value of $K_0 = 370^{+130}_{-95}$ keV cm^2 ($\chi^2_\nu = 9.69/12 = 0.81$). This is consistent with the best fit for the whole sample. Fitting only high-redshift ($z > 0.3$) clusters, we find a best-fit value of $K_0 = 220^{+100}_{-70}$ keV cm^2 ($\chi^2_\nu = 7.64/5 = 1.53$). Therefore, there is only a marginal statistical difference between the best-fit values of K_0 from the low- and high-redshift clusters. A very similar result is deduced from an examination of the $S_{\nu,\mathrm{arc}}/f_\nu$-$T_X$ relation (which is not as sensitive as the y_0-T_X relation to the entropy floor; MBHB03), where the low-redshift clusters are best fitted by entropy floor models with $K_0 \sim 300$ keV cm^2 while the high-redshift clusters are best fitted by entropy floor models with $K_0 \sim 200$ keV cm^2.

3.5. *The SZ Effect–L_X Relations*

The theoretical y_0-L_X relations have the interesting properties that they do not evolve strongly with redshift and, more importantly, are virtually insensitive to the presence of an entropy floor. The reason why this happens to be the case is not because the individual quantities, y_0 and L_X, are unaffected by an entropy floor (on the contrary, they are greatly modified), but because they are both affected in a

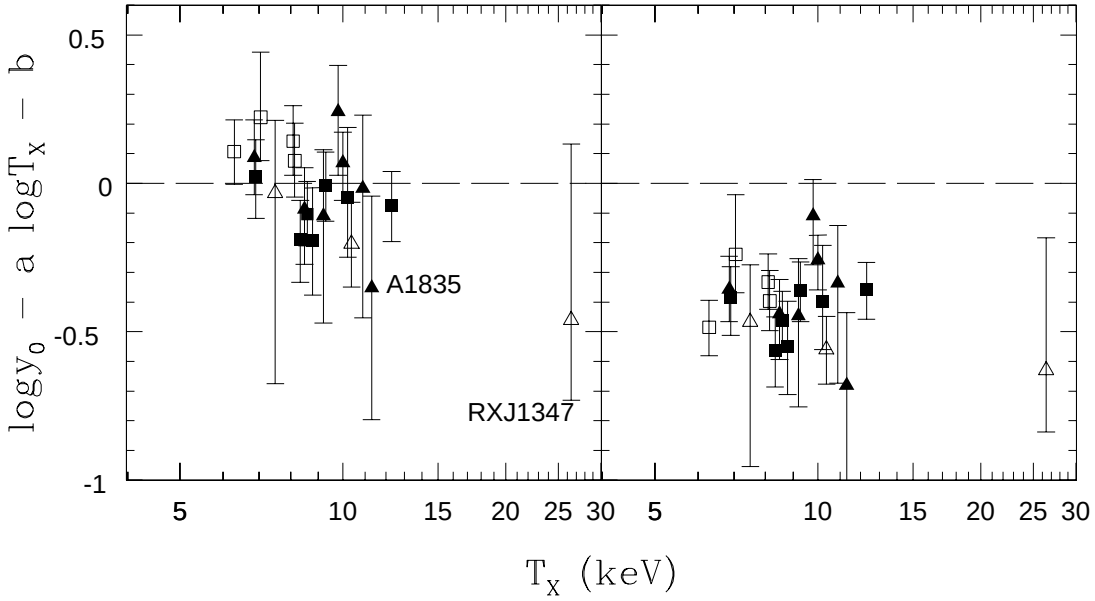


FIG. 5.—Residual plots for the y_0-T_X relation. *Left:* Residuals from a comparison between the entropy floor model with $K_0 = 300$ keV cm^2 and the observational data ($\chi^2_\nu = 1.32$). Neglecting A1835 and RX J1347.5−1145, we find a best fit of $K_0 = 305$ keV cm^2 with $\chi^2_\nu = 1.24$. *Right:* Residuals from a comparison between the self-similar model and the observational data ($\chi^2_\nu = 21.41$). The symbols have the same meaning as in Fig. 1. For clarity, error bars for the abscissa are not displayed.

very similar manner. Therefore, this correlation is less than ideal when it comes to probing the nongravitational entropy of galaxy clusters. However, the relation is still of great interest because it provides a valuable consistency check of the other scaling relations studied here.

Figure 6 is a plot of the observed y_0-L_X relation. This is superimposed on the predicted $z = 0.2$ (*thick lines*) and 0.5 (*thin lines*) relations for the self-similar model (*dotted line*) and the $K_0 = 100$ (*short-dashed line*), 300 (*long-dashed line*), 500 (*dot-dashed line*), and 700 keV cm^2 (*solid line*) entropy floor models. Since the theoretical y_0-L_X relations do not evolve strongly with redshift (compare the thin and thick lines), a qualitative " by eye " comparison is possible.

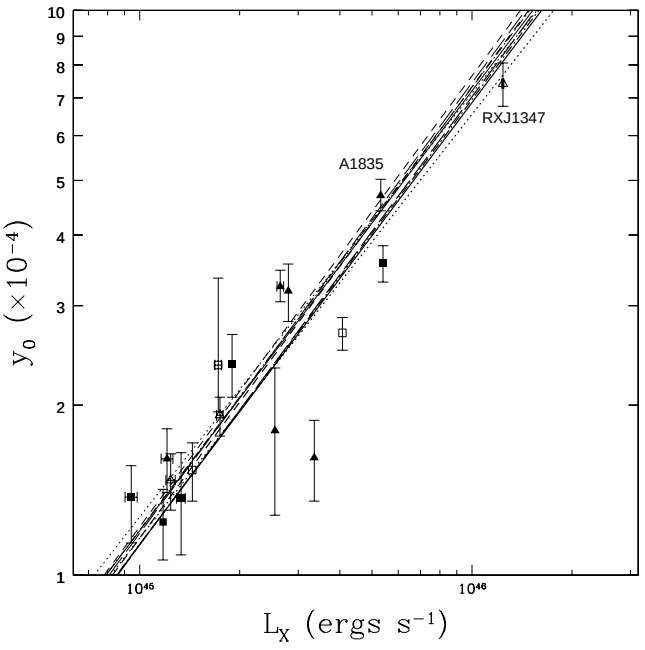


FIG. 6.—Observed and predicted y_0-L_X relations. The symbols have the same meaning as in Fig. 1. The dotted, short-dashed, long-dashed, dot-dashed, and solid lines represent the self-similar and $K_0 = 100$, 300, 500, and 700 keV cm^2 entropy floor models, respectively. Thin lines are for $z = 0.2$, and thick lines are for $z = 0.5$.

A clear correlation between a cluster's central Compton parameter and its bolometric X-ray luminosity is apparent in Figure 6. The relation is quite tight and follows the predicted trends. Even the two massive cooling flow clusters A1835 and RX J1347.5−1145 seem to follow the predicted trends. Thus, the observed y_0-L_X relation gives us confidence that our general understanding of the ICM is basically correct. That being said, the quality of the fit is not great in a statistical sense ($\chi^2_\nu = 67.36/16 = 4.21$). The high value of χ^2_ν undoubtedly arises from the random scatter present in the observed relation. The presence of this scatter may be inconsistent with theoretical predictions. We note, however, that observational systematic uncertainties for y_0 and L_X are on the order of 10% each (Reese et al. 2002). In addition, Mushotzky & Scharf (1997) have found that estimates of the X-ray luminosities of clusters can vary from study to study by up to 20%, most likely attributable to different measurement techniques. Conservatively estimating the *total* uncertainty on L_X to be 20%, we find a significantly improved fit of $\chi^2_\nu = 19.76/16 = 1.24$. As expected, the entropy floor level is not constrained by the data.

While the y_0-L_X relation is insensitive to the entropy floor level, the $S_{\nu,\mathrm{arc}}/f_\nu$-$L_X$ relation is not. Fitting all 15 clusters for which we have estimates of both the luminosity and SZ effect flux density, we find a best-fit entropy floor level of $K_0 = 310^{+70}_{-70}$ keV cm^2. However, the fit is not a good one, as is evident from the residuals plotted in Figure 7 and the calculated reduced χ^2 ($\chi^2_\nu = 34.34/14 = 4.27$). The two massive cooling flow clusters A1835 and RX J1347.5−1145 are obvious outliers. Ignoring these two clusters, we obtain $K_0 = 385^{+75}_{-70}$ keV cm^2 (2 σ error bars) and a significantly improved fit ($\chi^2_\nu = 13.79/12 = 1.15$). This best-fit value of

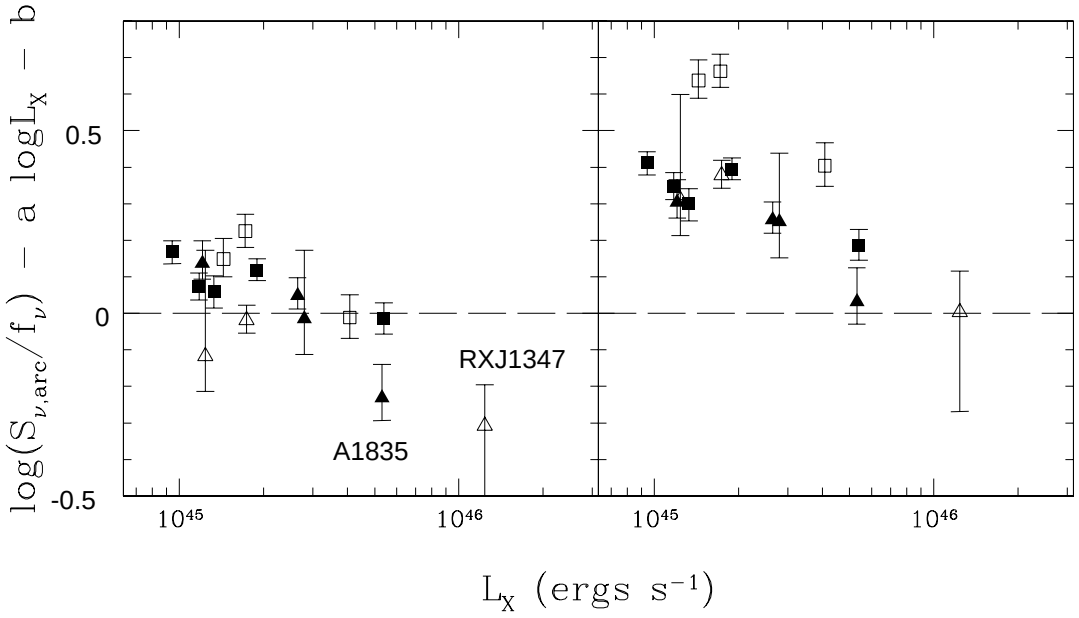


FIG. 7.—Residual plots for the $S_{\nu,\mathrm{arc}}/f_\nu$-$L_X$ relation. *Left:* Residuals from a comparison between the entropy floor model with $K_0 = 310$ keV cm^2 and the observational data ($\chi^2_\nu = 4.27$). Neglecting the two massive "cooling flow" clusters, A1835 and RX J1347.5−1145, we converge on $K_0 = 385$ keV cm^2 as the best-fit model with $\chi^2_\nu = 1.15$. *Right:* Residuals from a comparison between the self-similar model and the observational data ($\chi^2_\nu = 17.30$). The symbols have the same meaning as in Fig. 1. For clarity, error bars for the abscissa are not displayed.

K_0 is consistent with the results of §§ 3.2 and 3.3 and also with X-ray observations of nearby massive clusters. Splitting the sample into two redshift bins (<0.3 and >0.3), we also find there to be no difference in the entropy floors of "nearby" and "distant" galaxy clusters. This is the same as was found for the $S_{\nu,\mathrm{arc}}/f_\nu$-$y_0$ relation.

3.6. *Summary of Scaling Relations*

Every single SZ effect scaling relation that we have examined is consistent with or requires a high value for the entropy floor level, K_0. In fact, several of the trends, such as the y_0-T_X, y_0-$M(r_{500})$, and $S_{\nu,\mathrm{arc}}/f_\nu$-$y_0$ relations, rule out the standard self-similar model at many sigma. Neither of the relations shows any convincing evidence for strong evolution in K_0 out to the limit to which our sample extends ($z \sim 0.7$).

It is interesting that the estimates of K_0 from the various relations do not always agree. For example, the best-fit entropy floors from the y_0-T_X and $S_{\nu,\mathrm{arc}}/f_\nu$-$T_X$ trends are consistent with results from studies of X-ray scaling relations of nearby massive clusters (e.g., Babul et al. 2002) and the results of our SZ effect–luminosity relations but are marginally lower than the results from our $S_{\nu,\mathrm{arc}}/f_\nu$-$y_0$ and y_0-$M(r_{500})$ relations. A conservative estimate of the *true* value of K_0, however, must fall in between the results of each of the individual relations, i.e., 300 keV cm$^2 \lesssim K_0 \lesssim 600$ keV cm^2. This is clearly illustrated in Figure 8 through a plot of $\Delta\chi^2$ versus K_0 for the relations we have examined ($\Delta\chi^2 \equiv \chi^2 - \chi^2_{\mathrm{BF}}$, where χ^2_{BF} is the χ^2 for the best-fit power-law model for each of the scaling relations). A naive simultaneous fit to all of the relations, ignoring correlated variables and errors, yields $K_0 = 430^{+60}_{-55}$ keV cm^2 (99% level), which is remarkably similar to that derived solely from X-ray data (see Babul et al. 2002).

At present, it is unclear why some of the scaling relations do not converge on the same value of K_0. A more detailed analysis of this would require taking into account all of the observational and analysis biases (associated with both X-ray and SZ effect), which is beyond the scope of this paper. We expect that it will be possible to get a much more firm handle on these differences in the near future. First, the number of high-redshift clusters observed through the SZ effect is increasing rapidly (see Reese et al. 2002), and with it

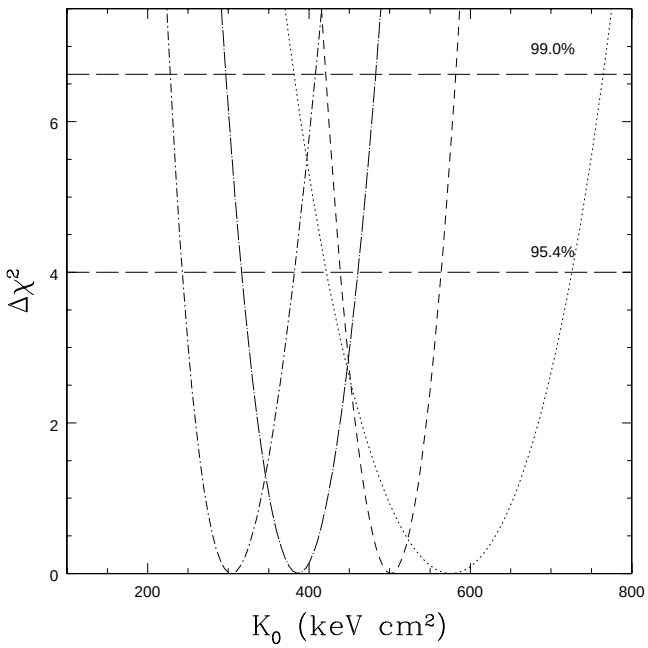


FIG. 8.—Constraints on K_0. The dot–short-dashed, dot–long-dashed, dashed, and dotted lines represent the y_0-T_X, $S_{\nu,\mathrm{arc}}/f_\nu$-$L_X$, y_0-$M(r_{500})$, and $S_{\nu,\mathrm{arc}}/f_\nu$-$y_0$ relations (the four most entropy floor–sensitive relations), respectively. The cooling flow clusters A1835 and RX J1347.5−1145 have been excluded from the fits.

comes improved statistics. Second, and perhaps more important, a number of new experiments (or substantial upgrades to existing ones) are already under construction and will greatly improve the quality of the SZ effect observations. For example, the bandwidths of the future SZA and the upgraded OVRO array are expected to be nearly an order of magnitude larger than that of current interferometers and, as such, will lead to substantial improvements in the signal-to-noise ratios of SZ effect data. Tighter constraints on the SZ effect surface brightness profiles of clusters will then be possible, and, in turn, more stringent limits can be placed on the entropy distributions of these clusters. Indeed, we demonstrate below that observations with the SZA and the upgraded OVRO array will allow one to constrain the amount of excess entropy in clusters all the way out to $z \sim 2$ and, best of all, without the need for any X-ray results.

4. THE FUTURE: OBSERVATIONS WITH SZA/OVRO

It was briefly discussed in § 3.1 that current SZ effect data alone cannot tightly constrain the three parameters of the surface brightness β model. A large degeneracy is present in the shape parameters, β and θ_c (e.g., Carlstrom et al. 1996; Grego et al. 2000, 2001). A number of authors have dealt with this problem by using the values of β and θ_c obtained from modeling the *X-ray* surface brightness of the cluster (e.g., Patel et al. 2000; Grainge et al. 2002a, 2002b; LaRoque et al. 2003). In the case of low/intermediate-redshift clusters, X-ray observations provide tighter constraints on these parameters than do SZ effect observations. However, a truly X-ray–independent probe of the ICM requires that only SZ effect data be used in the analysis. By using a joint maximum likelihood fit to both the X-ray and SZ effect surface brightnesses of clusters, Reese et al. (2000, 2002) found a compromise between these two scenarios. Pushing the analysis of the ICM to higher redshifts than considered by Reese et al. (2000, 2002), however, will likely bring us into a regime that is uniquely accessible to SZ effect observations. Fortunately, substantial upgrades are planned for currently operational arrays (for example, the current BIMA and OVRO arrays are being upgraded and merged into the Combined Array for Research in Millimeter-Wave Astronomy[5] [CARMA]), and a number of new interferometers are planned as well (e.g., SZA,[6] AMiBA, and AMI; Holder et al. 2000; Lo et al. 2000; Kneissl et al. 2001). These experiments will substantially improve the quality of SZ effect observations. Below we compare the expected performance of the SZA and the (soon to be) upgraded OVRO array with the currently operational BIMA/OVRO arrays. We show that the degeneracy in the β-θ_c plane is greatly reduced with data from the SZA or the upgraded OVRO array and this will allow for accurate determinations of y_0 and S_ν, without the need for any X-ray results.

4.1. *Mock Observations*

To compare the arrays, we first generate "mock" observations of model galaxy clusters. We follow a method similar to that outlined by Holder et al. (2000). First, we create a Compton parameter map, $y(\theta_x, \theta_y)$, for each model cluster. These maps are converted into SZ effect intensity decrement maps. Before we can do this, however, we must assume an observing frequency for each of the interferometers. The current BIMA and OVRO arrays use amplifiers that operate over the range 26–36 GHz (Reese et al. 2000). We assume a frequency centered on 30 GHz for these arrays. The upgraded OVRO array and the SZA are expected to have amplifiers that operate at 26–36 GHz and at 85–115 GHz. We assume frequencies centered on 30 and 90 GHz for these arrays. Thus, we generate six different decrement maps for each model cluster: 30 GHz maps for the current BIMA/OVRO arrays and 30 and 90 GHz maps for the SZA and upgraded OVRO array.

Interferometers do not image the sky. Rather, they measure the Fourier transform of the SZ effect intensity decrement multiplied by the primary beam. A particular value of this observable is referred to as a "visibility" and is given by

$$V(u,v) = j_\nu \int y(\theta_x, \theta_y) A(\theta_x, \theta_y) e^{2\pi i (u\theta_x + v\theta_y)} d\theta_x \, d\theta_y \, , \quad (8)$$

where u and v are the conjugate variables, θ_x and θ_y are the projected sky coordinates, and $A(\theta_x, \theta_y)$ is the primary beam. At 30 GHz, the sensitivity patterns for the primary beams of the BIMA and OVRO arrays (both current and upgraded) and the SZA are, or will be, well represented by Gaussians with FWHM $\approx 6\farcm6$, $4\farcm2$, and $10'$–$12'$, respectively. We assume FWHM $= 10\farcm8$ for the SZA. For more on the above formalism see White et al. (1999).

We multiply the SZ effect maps by the Gaussian primary beams described above and Fourier transform the result. We discard all visibilities for baselines $[R_{u,v} \equiv (u^2 + v^2)^{1/2}]$ that are not probed by these interferometers. At 30 GHz, the BIMA and OVRO arrays probe multipole moments of $\ell = 2\pi R_{u,v} \gtrsim 4000$ and 7000, respectively. We assume uniform coverage over the ranges $4200 \lesssim \ell \lesssim 20,000$ and $7200 \lesssim \ell \lesssim 20,000$ for these arrays, respectively. The smaller 3.5 m dishes of the SZA will be able to probe shorter baselines (larger angular scales) and are expected to sample $\ell \gtrsim 2000$. We assume uniform coverage over the range $2400 \lesssim \ell \lesssim 20,000$ (also at 30 GHz).

Finally, we add random Gaussian noise to each of the mock observations. At 30 GHz, we assume system temperatures (scaled to the atmosphere) of 45 K for the BIMA and OVRO arrays and 30 K for the SZA. At 90 GHz, we assume system temperatures of 100 K for the SZA and for the upgraded OVRO array. The current BIMA/OVRO arrays have effective noise bandwidths of approximately 550/1000 MHz, while both the upgraded OVRO array and the SZA are expected to have bandwidths of 8 GHz. A total integration time of 40 hr is assumed for each of the arrays at both 30 and 90 GHz. For specificity, the mock observations for the current BIMA and OVRO arrays have rms noise levels of approximately 150 and 70 μJy beam^{-1}, respectively, while the upgraded OVRO array has noise levels of 25 and 50 μJy beam^{-1} at 30 and 90 GHz, respectively, and the *SZA* has noise levels of 40 and 140 μJy beam^{-1} at 30 and 90 GHz, respectively.

4.2. *Analyzing the Mock Observations*

To analyze the mock observations, we follow the method described in a number of observational papers based on

[5] For information on CARMA see http://www.mmarray.org.

[6] For information on SZA see http://astro.uchicago.edu/sze/survey.html.

genuine BIMA/OVRO data (e.g., Carlstrom et al. 1996; Grego et al. 2000, 2001; Reese et al. 2000, 2002; Joy et al. 2001; LaRoque et al. 2003). We model the observations with the isothermal β models.[7] We create model SZ effect maps for various choices of the three free parameters (y_0, θ_c, and β), multiply the maps by the appropriate primary beams, Fourier transform the maps, and compare the results to the mock observations in § 4.1 via a χ^2 statistic. The best-fit parameters are those that result in the minimum value of χ^2. Note that the comparisons between the β models and the mock observations are done in the Fourier domain (also referred to as the u-v plane), where the noise characteristics and spatial filtering of the interferometers are well understood. Like the observers, we do not "deconvolve" the mock observations for analysis.

To demonstrate the quality of the data to be produced by the SZA and the upgraded OVRO array, we plot in Figure 9 confidence contours for the β and θ_c parameters from "observations" of a $T_X = 6.7$ keV ($M_{tot} \approx 5.6 \times 10^{14}\ M_\odot$) cluster at $z = 1$. The third free parameter, y_0, is allowed to assume its best-fit value at each pair of β and θ_c (i.e., the plot is a projection of the confidence "volume" onto the β-θ_c plane). The contours correspond to a $\Delta\chi^2$, and the filled squares indicate the best-fit models. The projection of the $\Delta\chi^2 = 1$ line onto the axes gives the 68% confidence interval for each of the two parameters. The contour labeled "current" is the result of fitting the SZ effect surface brightness model to the mock observations with the currently operational BIMA/OVRO arrays (both arrays have similar sensitivity patterns). The contours labeled "SZA" and "OVRO" are the results of simultaneously fitting the surface brightness model to the mock 30 and 90 GHz SZA observations and the mock 30 and 90 GHz upgraded OVRO observations, respectively. Lastly, the contour labeled "SZA+OVRO" is the result of simultaneously fitting all four upgraded OVRO and SZA mock observations.

[7] Note that we do not assume that the model cluster used to make the mock observations is necessarily isothermal.

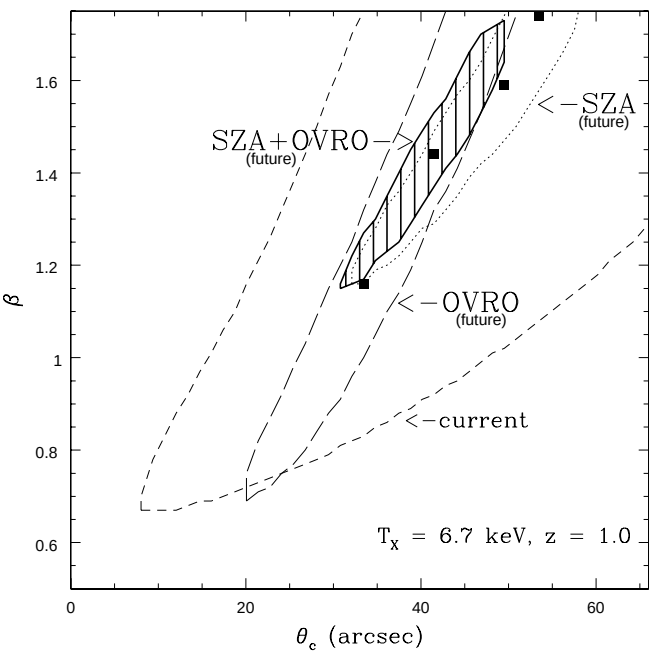


FIG. 9.—Comparison of constraints on the surface brightness profile of a distant, massive cluster. The filled squares indicate the best-fit parameters from modeling "mock" observations of the model cluster (the square at $\beta = 1.74$ is for "current" data, while the square at $\beta = 1.59$ is for "SZA" data). The contours give the 68% confidence regions on the two parameters ($\Delta\chi^2 = 1$). The normalization, y_0, is allowed to assume its best-fit value at each point in the plot (see text).

First, it is obvious that the "current" mock observational data do not tightly constrain β and θ_c and, furthermore, these parameters are strongly correlated, as found when modeling genuine BIMA/OVRO data (see, e.g., Fig. 3 of Grego et al. 2000; Fig. 2 of Grego et al. 2001). This gives us confidence that we have produced realistic mock observations. The large degeneracy in the β-θ_c plane is why a number of authors elect to use X-ray constraints on these parameters instead or, in the case of Reese et al. (2000, 2002), use a simultaneous fit to both X-ray and SZ effect data. However, data from the upcoming SZA and the upgraded OVRO array will be able to place much tighter constraints on these parameters (compare the "OVRO" and "SZA" contours with the "current" contour). Note that the correlation between β and θ_c remains for the SZA and OVRO "data," but its size has been dramatically reduced. A simultaneous fit to both the SZA and upgraded OVRO data yields even better constraints on these parameters (*shaded region*).

To get an idea of how well the future SZ effect data can constrain K_0, the entropy floor level, we use the 68% confidence volume (β, θ_c, y_0) for the "SZA+OVRO" contour to "measure" y_0 and $S_{\nu,arc}/f_\nu$. The inferred statistical uncertainty associated with the central Compton parameter and integrated SZ effect flux density within the central 1′ for this cluster is only about 10% and 15%, respectively. Comparing this to the predicted $S_{\nu,arc}/f_\nu$-y_0 relations (Fig. 2 of MBHB03), it should, therefore, be possible to constrain the entropy floor level of this cluster to within 50–75 keV cm^2 or so. This is comparable with statistical uncertainties associated with X-ray measurements of nearby clusters. This is remarkable considering that no X-ray "data" were used in the analysis and the cluster lies at $z = 1$. We also find that reasonably accurate measurements of K_0 are possible for clusters all the way out to $z \sim 2$.

The SZA and upgraded OVRO array will be excellent tools for probing the nongravitational entropy of distant clusters. Because X-ray data will not be required to constrain the shapes of the SZ effect surface brightness profiles of clusters observed with these planned interferometers, comparisons of data to predicted scalings (such as $S_{\nu,arc}/f_\nu$-y_0) will provide *independent* constraints on the properties of the intracluster gas. It will then also be possible to take advantage of the redshift independence of the SZ effect and monitor the evolution of nongravitational processes in clusters right back to the epoch of cluster formation itself.

5. DISCUSSION

Up until now, measurements (both direct and indirect) of the entropy floors of massive galaxy clusters have been limited to X-ray observations. Furthermore, these past X-ray studies have generally focused on nearby ($z \sim 0$) clusters, and, as such, little is known about the evolution of the entropy floor (and the nongravitational processes that produce it) with cosmic time. In the companion paper we explored the extent to which the thermal SZ effect is

modified by the presence of an entropy floor. Because it depends differently on the temperature and density of ICM and, also, because it is redshift independent, the SZ effect could potentially be a very powerful, independent test of the entropy floors of even the most distant galaxy clusters.

The central focus of the present paper was to compare our theoretical relations from MBHB03 (including one that can potentially be measured through SZ effect observations only) to available high-redshift SZ effect data from the literature to determine if the SZ effect data support the presence of an entropy floor and, if so, how does the inferred level of that floor compare with that required to match local X-ray trends. This is the first time such a comparison has been done, and we have made use of the largest compilation of high-z SZ effect clusters to date. A detailed analysis of seven different SZ effect scaling relations indicates that the entropy floor in clusters with $0.14 \lesssim z \lesssim 0.78$ is between 300 keV cm^2 $\lesssim K_0 \lesssim$ 600 keV cm^2, and there are no strong indications for evolution in K_0 over that redshift interval. Our estimate for the value of K_0 is remarkably similar to that derived from studies of X-ray scaling relations of nearby ($z \sim 0$) massive clusters, which suggest that $K_0 \gtrsim 300$ keV cm^2 (e.g., Tozzi & Norman 2001; Babul et al. 2002; McCarthy et al. 2002).

At present, the source (or sources) of the "excess" entropy is still not known. What constraints can be placed on the possible sources by the results of the present study? First, as in previous studies of X-ray scaling relations, our analysis indicates that the entropy of the ICM has been significantly raised by some nongravitational process(es). In terms of thermal energy, this corresponds to a few keV per particle for massive clusters. This means that supernova explosions probably cannot be the sole contributor to the entropy floor, since they are expected to impart $\lesssim$0.3 keV particle^{-1} (e.g., Valageas & Silk 1999; Balogh et al. 1999; Wu et al. 2000). This was previously known, but the present study, which offers an independent examination of the ICM, reinforces this conclusion. Recently, it has been speculated that quasar outflows could be the source of the excess entropy (e.g., Nath & Roychowdhury 2002). The entropy requirements deduced in the present study (and previous X-ray studies) are probably met by quasar outflows, but it is not yet known what mechanism (if any) couples the outflows to the ambient ICM. Alternatively, and somewhat paradoxically, radiative cooling has also been shown to raise the mean entropy of the ICM. It is possible that cooling in combination with supernovae and/or quasar outflows could be responsible for the observed SZ effect and SZ effect–X-ray relations. Whatever the source may be, it must reproduce the fact that K_0 does not change significantly out to $z \sim 0.7$. It could well be that this trend will become a critical piece of information for discriminating between the various theoretical models currently being proposed. An unchanging value of K_0 with redshift is obviously consistent with the generic "preheating" scenario; however, it remains to be seen whether it is consistent with more realistic heating models that distribute entropy nonuniformly and over an extended period of time. Without a detailed analysis, it is difficult to say whether or not it is consistent with radiative cooling contributing significantly to the excess entropy. We are currently in the process of examining the effects of radiative cooling on SZ effect scaling relations (see the discussion in MBHB03).

Current SZ effect data cannot tightly constrain the surface brightness profiles of clusters. This prevents the SZ effect from being used as an independent (of X-ray) probe of the entropy floor and the ICM in general. Thus, any advantages that the SZ effect has over the X-ray emission (e.g., redshift independence) are severely diminished because X-ray data are needed to help constrain the shape of the surface brightness profiles. Therefore, an additional aim was to examine the ability of the next generation of SZ effect experiments to probe nongravitational entropy in distant clusters. We have shown that the SZA and the upgraded OVRO array will produce high signal-to-noise ratio data that will allow one to tightly constrain the surface brightness profiles of even very distant clusters and without the need for any X-ray results. As in the present study, these surface brightness profiles can then be compared to theoretical predictions in order to place stringent constraints on the level of the entropy floor. It will be very interesting to see if the trend of constant K_0 (with redshift) deduced here holds up and, if so, to determine how far back in redshift it extends.

Aside from the appearance and structure of individual clusters, our work has implications for universal SZ effect quantities, such as the SZ effect angular power spectrum, SZ effect cluster source counts, and the mean Compton parameter of the universe. These quantities can be used to measure cosmological parameters and test cluster formation scenarios (see Carlstrom, Holder, & Reese 2002 for a comprehensive review). A number of studies have already examined how nongravitational gas physics modifies these quantities (e.g., Holder & Carlstrom 2001; Cavaliere & Menci 2001; da Silva et al. 2001; Springel, White, & Hernquist 2001; White, Hernquist, & Springel 2002). However, none of these studies have invoked entropy injection at the high level estimated in the present analysis. Generally, low levels of entropy injection ($K_0 \sim 100$ keV cm^2), which are consistent with X-ray measurements from low-mass groups (Ponman et al. 1999), were implemented. We are in the process of investigating how the power spectrum, source counts, and mean Compton parameter are modified by higher initial entropies.

We thank Erik Reese for making available his SZ effect data prior to publication. We also thank Ann Gower, John Carlstrom, Peng Oh, Kathy Romer, and Mark Voit for helpful discussions. A. B. would like to acknowledge the hospitality extended to him by the Canadian Institute for Theoretical Astrophysics during his tenure as CITA Senior Fellow. I. G. M. is supported by a postgraduate scholarship from the Natural Sciences and Engineering Research Council of Canada (NSERC). A. B. is supported by an NSERC operating grant, G. P. H. is supported by the W. M. Keck Foundation, and M. L. B. is supported by a PPARC rolling grant for extragalactic astronomy and cosmology at the University of Durham.

REFERENCES

Allen, S. W. 1998, MNRAS, 296, 392
———. 2000, MNRAS, 315, 269
Allen, S. W., & Fabian, A. C. 1998, MNRAS, 297, L57
Babul, A., Balogh, M. L., Lewis, G. F., & Poole, G. B. 2002, MNRAS, 330, 329
Balogh, M. L., Babul, A., & Patton, D. R. 1999, MNRAS, 307, 463
Bower, R. G. 1997, MNRAS, 288, 355
Borgani, S., et al. 2001, ApJ, 559, L71
Bryan, G. L. 2000, ApJ, 544, L1
Cantalupo, C. M., et al. 2003, ApJ, submitted

Carlstrom, J. E., Holder, G. P., & Reese, E. D. 2002, ARA&A, 40, 643
Carlstrom, J. E., Joy, M., & Grego, L. 1996, ApJ, 456, L75
Cavaliere, A., & Fusco-Femiano, R. 1976, A&A, 49, 137
———. 1978, A&A, 70, 677
Cavaliere, A., & Menci, N. 2001, MNRAS, 327, 488
Clowe, D., & Schneider, P. 2001, A&A, 379, 384
Cotter, G., et al. 2002, MNRAS, 334, 283
da Silva, A. C., et al. 2001, ApJ, 561, L15
Davé, R., Katz, N., & Weinberg, D. H. 2002, ApJ, 579, 23
Ettori, S., & Fabian, A. C. 1999, MNRAS, 305, 834
Evrard, A. E., & Henry, J. P. 1991, ApJ, 383, 95
Fixsen, D. J., et al. 1996, ApJ, 473, 576
Grainge, K., et al. 2002a, MNRAS, 329, 890
———. 2002b, MNRAS, 333, 318
Grego, L., et al. 2000, ApJ, 539, 39
———. 2001, ApJ, 552, 2
Herbig, T., et al. 1995, ApJ, 449, L5
Holder, G. P., & Carlstrom, J. E. 2001, ApJ, 558, 515
Holder, G. P., et al. 2000, ApJ, 544, 629
Holzapfel, W. 1996, Ph.D. thesis, Univ. California, Berkeley
Holzapfel, W., et al. 1997, ApJ, 480, 449
———. 2000, ApJ, 539, 57
Hughes, J. P., & Birkinshaw, M. 1998, ApJ, 501, 1
Itoh, N., Kohyama, Y., & Nozawa, S. 1998, ApJ, 502, 7
Jones, M., et al. 1993, Nature, 365, 320
———. 2003, MNRAS, submitted
Joy, M., et al. 2001, ApJ, 551, L1
Kaiser, N. 1991, ApJ, 383, 104
Kneissl, R., et al. 2001, MNRAS, 328, 783
Komatsu, E., et al. 1999, ApJ, 516, L1
Lamarre, J. M., et al. 1998, ApJ, 507, L5
LaRoque, S. J., et al. 2003, ApJ, submitted
Lloyd-Davies, E. J., Bower, R. G., & Ponman, T. J. 2002, MNRAS, submitted
Lloyd-Davies, E. J., Ponman, T. J., & Cannon, D. B. 2000, MNRAS, 315, 689
Lo, K. Y., et al. 2000, in IAU Symp. 201, New Cosmological Data and the Values of the Fundamental Parameters, ed. A. Lasenby & A. Wilkinson (San Francisco: ASP), 31
Machacek, M. E., et al. 2002, ApJ, 567, 188
Markevitch, M. 1998, ApJ, 504, 27
Markevitch, M., & Vikhlinin, A. 2001, ApJ, 563, 95
Mason, B. S., Myers, S. T., & Readhead, A. C. S. 2001, ApJ, 555, L11
Mauskopf, P. D., et al. 2000, ApJ, 538, 505
McCarthy, I. G., Babul, A., & Balogh, M. L. 2002, ApJ, 573, 515
McCarthy, I. G., Babul, A., Holder, G. P., & Balogh, M. L. 2003, ApJ, 591, 526
Miralda-Escudé, J., & Babul, A. 1995, ApJ, 449, 18
Mushotzky, R. F., & Scharf, C. A. 1997, ApJ, 482, L13
Myers, S. T., et al. 1997, ApJ, 485, 1
Nath, B. B., & Roychowdhury, S. 2002, MNRAS, 333, 145
Navarro, J. F., Frenk, C. S., & White, S. D. M. 1997, ApJ, 490, 493
Novicki, M. C., Sornig, M., & Henry, J. P. 2002, AJ, 124, 2413
Nozawa, S., et al. 2000, ApJ, 536, 31
Ota, N., et al. 2002, in IAU 8th Asian-Pacific Regional Meeting, Proc. Vol. 1, ed. S. Ikeuchi, J. Hearnshaw, & T. Hanawa (San Francisco: ASP), 465
Patel, S. K., et al. 2000, ApJ, 541, 37
Pointecouteau, E., et al. 1999, ApJ, 519, L115
———. 2001, ApJ, 552, 42
———. 2002, A&A, 387, 56
Ponman, T. J., Cannon, D. B., & Navarro, J. F. 1999, Nature, 397, 135
Press, W. H., Teukolsky, S. A., Vetterling, W. T., & Flannery, B. P. 1992, Numerical Recipes in Fortran: The Art of Scientific Computing (Cambridge: Cambridge Univ. Press)
Reese, E. D., et al. 2000, ApJ, 533, 38
———. 2002, ApJ, 581, 53
Saunders, R., et al. 2003, MNRAS, in press
Springel, V., White, M., & Hernquist, L. 2001, ApJ, 549, 681
Sunyaev, R., & Zeldovich, Y. 1970, Comments Astrophys. Space Phys., 2, 66
———. 1980, MNRAS, 190, 413
Thomas, P. A., et al. 2002, MNRAS, 330, L48
Tozzi, P., & Norman, C. 2001, ApJ, 546, 63
Valageas, P., & Silk, J. 1999, A&A, 350, 725
Vikhlinin, A., et al. 2002, ApJ, 578, L107
Voit, M. G., & Bryan, G. L. 2001, Nature, 414, 425
Voit, M. G., Bryan, G. L., Balogh, M. L., & Bower, R. G. 2002, ApJ, 576, 601
White, D. A. 2000, MNRAS, 312, 663
White, D. A., Jones, C., & Forman, W. 1997, MNRAS, 292, 419
White, M., Hernquist, L., & Springel, V. 2002, ApJ, 579, 16
White, M., et al. 1999, ApJ, 514, 12
Wu, K. K. S., Fabian, A. C., & Nulsen, P. E. J. 2000, MNRAS, 318, 889
Wu, X.-P., & Fang, L. Z. 1997, ApJ, 483, 62